RESEARCH ARTICLE

Chao SHEN, Wei GU, Enbo LUO

Transient performance comparison of grid-forming converters with different FRT control strategies

© Higher Education Press 2022

Abstract Grid-forming converters (GFMs) are faced with the threat of transient inrush current and synchronization instability issues when subjected to grid faults. Instead of disconnecting from the grid unintentionally, GFMs are required to have fault ride through (FRT) capability to maintain safe and stable operation in grid-connected mode during grid fault periods. In recent studies, different FRT control strategies with distinguishing features and that are feasible for different operation conditions have been proposed for GFMs. To determine their application scope, an intuitive comparison of the transient performance of different FRT control strategies is presented in this paper. First, three typical FRT control strategies (virtual impedance, current limiters, and mode-switching control) are introduced and transient mathematical models are established. A detailed comparison analysis on transient inrush current and transient synchronization stability is then presented. The results will be useful for guiding the selection and design of FRT control strategies. Finally, simulation results based on PSCAD/EMTDC are considered to verify the correctness of the theoretical analysis.

Keywords grid-forming converters (GFMs), fault ride through (FRT), transient stability, transient inrush current, transient modeling

Chao SHEN (✉), Wei GU
School of Electrical Engineering, Southeast University, Nanjing 214135, China
E-mail: 101300120@seu.edu.cn

Enbo LUO
Electric Power Test and Research Institute, Yunnan Power Grid, Kunming 650032, China

1 Introduction

Voltage source converters (VSCs) are widely used as the interface to integrate renewable energy resources to the power system. The primary control objective of VSCs is generally to extract maximum power of renewable energy resources, such as wind turbine or photovoltaic resources, and adapt to dynamic responses of the grid voltage. To maintain synchronization with the grid, phase-lock loop (PLL) is commonly used in VSCs, which are usually referred as grid-following VSCs (GFLs) [1–2]. Along with the increasing integration of VSCs, VSCs are required to provide inertia supporting and voltage/frequency regulation capabilities to the power system, especially in islanded mode. Therefore, grid-forming VSCs (GFMs) are proposed, including droop-controlled VSCs and virtual synchronous generators (VSGs) [3–5]. Different from GFLs, GFMs are usually synchronized with an AC grid through power synchronization control (PSC). Droop-controlled VSCs can automatically realize active power sharing among multi-VSCs, and the concept of VSGs are proposed to mimic the dynamic response of synchronous generators (SGs) to provide extra inertia to the grid, which has attracted great attention [4–5].

Although GFMs have the advantages of providing frequency/voltage regulation to grid, they are faced with several technical issues, especially during grid fault periods. Because GMFs are controlled to mimic the dynamic response of SGs, transient inrush current will occur within several milliseconds for GFMs, which probably cause damage to semi-conductor devices due to their limited thermal capacity [1]. Moreover, GFMs are more prone to the transient synchronization instability caused by the power imbalance between reference active power and output active power during transient period [6–7]. According to the grid code [8–9], GFMs are required to maintain grid-connected operation to support the grid instead of disconnecting from the grid unintentionally, which calls for fault ride through (FRT) capability of GFMs. For example, distributed generators

(DGs) are required to remain in connection with the grid in Japan when the fault duration is less than 1 s and the voltage drop is larger than 20% of the rated value [9]. However, the introduction of different FRT control strategies makes the transient response of GFMs more complicated, which probably result in unpredictable transient instability issues. Thus, to promote the integration of GFMs, it is necessary to carry out transient performance comparison to give insights into the transient response of GFMs.

From the perspective of time domain, the FRT process can be divided into three successive stages [10], which is illustrated in Fig. 1, and different control targets need to be achieved at different stages.

1) Stage I: first several cycles after grid faults. During this stage, transient inrush current needs to be eliminated to protect semi-conductor devices instantaneously. For GFMs, inrush current elimination needs to be accomplished within ten milliseconds [1].

2) Stage II: fault sustaining stage. During this stage, GFMs should maintain synchronization with the grid to avoid stepping into unstable condition. According to the grid requirement, voltage/frequency support should be considered as well.

3) Stage III: recovery to normal operation after fault clearance. During this stage, GFMs should recover to the normal control strategy and avoid power oscillation. If converters are switched to current control mode during stage II, the GFMs are required to realize re-synchronization with the grid again.

As indicated in Fig. 1, it is important for GFMs to realize inrush current limitation at stage I and maintain transient stability at stage II. When the fault is cleared, GFMs need to re-synchronize with the grid as soon as possible at stage III. This is because both inrush current and transient instability issues will lead to the failure of FRT process and result in tripping of the GFMs. To date, the transient response of the GFMs throughout the FRT process has not been thoroughly discussed. In existing studies, different FRT control strategies have been proposed [11–20], such as mode-switching control (MSC) [11–12], virtual impedance control (VIC) [13–16], and internal current limiter control (CLC) [17–18]. A current-restraining method based on MSC was proposed in Ref.

[11], which involves varying the GFMs from voltage control mode to current control mode to regulate output current directly during grid fault periods. When the fault is cleared, the GFMs need to recover to the normal control mode and realize re-synchronization with the grid again, which is accomplished by introducing the concept of virtual line impedance. However, the re-synchronization capability of GFMs is sensitive to controller parameters, and the effect of virtual line impedance has not been revealed, which probably result in the continuous-oscillation phenomenon. In Ref. [14], virtual impedance is added to GFMs to limit fault current when grounded faults are detected. However, the inrush current elimination performance of VIC is limited in first several cycles due to the existence of an aperiodic fault current component [1]. Another method was proposed in Ref. [15], which shows that the GFMs can achieve fault current control via additional virtual admittance and adjustable virtual impedance [16]. However, it is questionable whether the transient response of this method is quick enough to deal with inrush current issues. Furthermore, inrush current limiting can be achieved by using inherent current limiters in voltage and current multiple control loops, since the reference current can be simply restrained by limiters [17]. However, the windup and latch-up introduced by limiters would reduce the stable operation domain and brings difficulties in the re-synchronization process [18]. Moreover, the output active power and reactive power of GFMs with CLC would be uncontrollable during the transient period.

In existing studies, other FRT control strategies have been established by controlling the output voltage. In Ref. [18], a novel control based on a predictive finite-set model was proposed, which can achieve overcurrent elimination and improve power quality during asymmetrical faults. However, it is necessary to obtain detailed system parameters that realize accurate prediction, and nonlinear characteristics add difficulties to the design of control parameters. Furthermore, voltage control loops can also be used to achieve FRT capability [20–21]. In these proposed control strategies, the reference voltage magnitude becomes limited when the fault current exceeds the threshold value [20] or the PI controller reaches its limit value [21]. However, it is
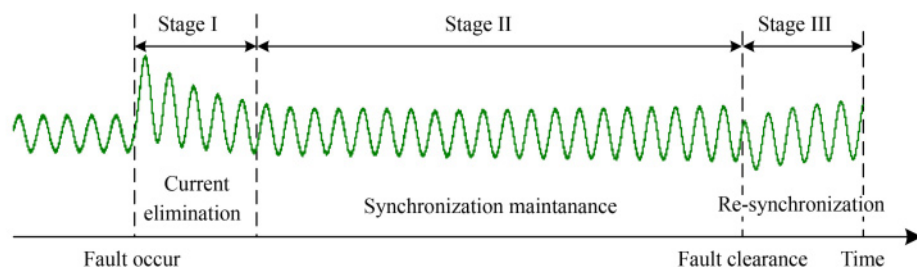
Fig. 1   Different stages of GFMs throughout the whole transient period.

questionable whether the proposed control can guarantee the stable operation after fault clearance. In all above literatures, although several control strategies are proposed to improve the FRT capability of GFMs, there is a lack of summary and comparison of current-limitation effects among different FRT control strategies. Moreover, these FRT control strategies take either current limitation or transient stability into consideration, though unexpected stability issues probably occur throughout the FRT process, especially in multi-GFM systems. Thus, it is necessary to determine the transient performance of typical FRT control to give insights into the transient stability mechanism of GFMs. The main contributions of this paper can be summarized as follows:

1) The transient inrush current of grid-forming converters is described, and the transient current elimination effects of three typical FRT control strategies are compared considering fault detection delay.

2) The transient synchronization stability of grid-forming converters with three different FRT control strategies are revealed using Equal Area Criterion (EAC) theory throughout the fault period. Based on the mechanism analysis, a control-parameter design for enhanced transient stability is presented.

In this paper, the comparison between the transient performance of GFMs and different FRT control strategies are performed from the perspectives of current limitation and transient stability maintenance. First, the principle of three typical FRT control strategies are introduced. Thereafter, transient current characteristics are described using mathematical analytic equations, and the current limitation effect is compared. Moreover, the effect of time delay on transient inrush current is analyzed. Furthermore, the transient synchronization

mechanism of GFMs throughout the FRT process is investigated, and a design-oriented transient stability analysis is performed.

2   Principles of typical FRT control strategies

The main circuit topology and three typical FRT control strategies of a grid-connected GFM is shown in Fig. 2. The control topology of the GFM under normal operation conditions can be divided into two parts: power control and voltage/current control. The power control part, which is based on Ref. [5], is adopted in this paper, and an active power control loop is designed to emulate the dynamic response of SGs to provide inertia and realize power sharing among multi-GFMs simultaneously, which can be described as follows:

$$J\frac{\mathrm{d}\omega}{\mathrm{d}t} = T_0 - T_{\mathrm{em}} - D_{\mathrm{p}}(\omega - \omega_0), \qquad (1)$$

where T_0 and T_{em} are the reference torque and electromagnetic torque, respectively. J and D_{p} represent for the virtual inertia and damping coefficient, respectively. Subscript p represents damping coefficient for active power regulation. ω_0 is the rated angular frequency. The reactive power control adopts Q-V droop characteristics to realize reactive power sharing among multi-GFMs, and its mathematical model can be represented as follows:

$$K\frac{\mathrm{d}E_d}{\mathrm{d}t} = Q_0 - Q - D_q(E_d - E_0), \qquad (2)$$

where D_q is the Q-V droop coefficient and K represents
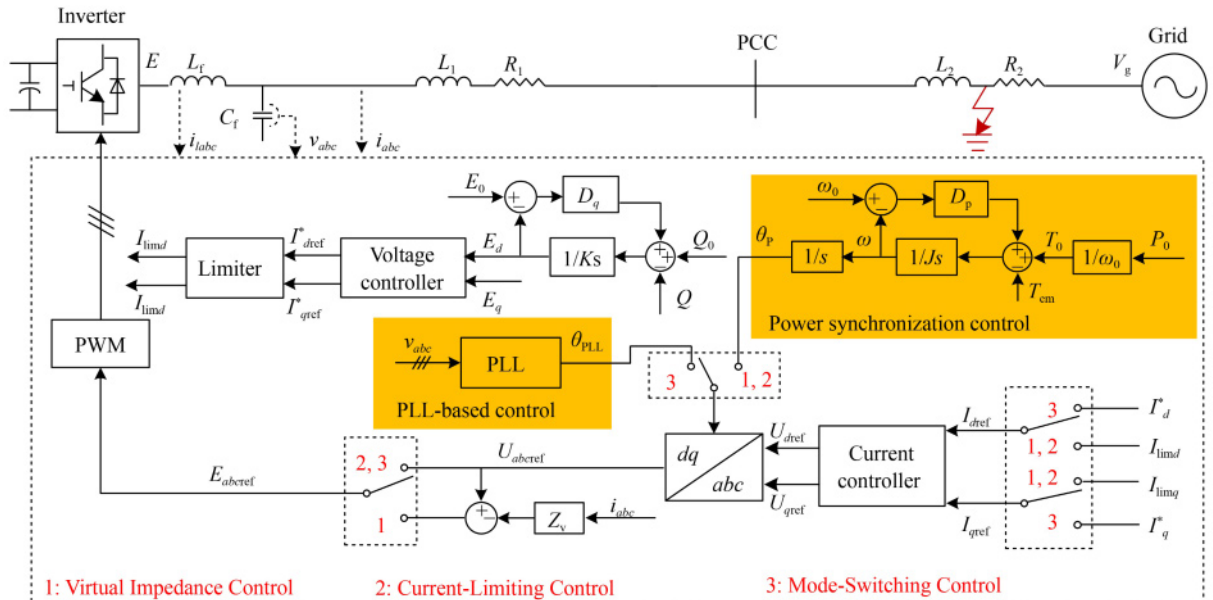

Fig. 2   Control block diagram of a GFM connected to a grid with three typical FRT control strategies.

the voltage integral coefficient. Subscript q represents damping coefficient for reactive power regulation. E_0 and Q_0 are the reference voltage and reference reactive power, respectively. E_d is output voltage in d axis. It can be seen from Fig. 2 that cascaded voltage and current control loops are accomplished using PI controller in the dq reference frame. The voltage control loop delivers reference current to the current control loop, and current limiters are inherently adopted in the current control loop to limit the reference current during grid fault periods. The generated reference voltage will be delivered to the pulse width modulation (PWM) module to drive semiconductor devices. When there is a grounded fault with the grid, FRT control strategies would be activated to limit the fault current. Three typical FRT control are considered in this paper, and the corresponding relationship between switchers S_1–S_3 and FRT control strategies is concluded in Table 1. Detailed control topologies will be introduced in the following sections.

2.1   Virtual Impedance Control (VIC)

As illustrated in Fig. 2, when switchers S_1–S_3 are chosen at 1, VIC will be adopted. By adding additional impedance Z_v, the reference voltage will be reduced, thereby preventing the voltage control loop from delivering excessive reference current to the control system [14]. The output current of the GFM in VIC mode can be regulated as follows:

$$i_{abc} = (V_{abc} - V_g)/(Z_{eq} + Z_v), \qquad (3)$$

where V_{abc} and V_g are the internal voltage of the GFM and grid voltage, respectively. Z_{eq} represents the equivalent impedance between the GFM and the grid, and Z_v is the added virtual impedance. i_{abc} represents the output current of the GFM. After fault clearance, the virtual impedance will be withdrawn to guarantee power sharing accuracy under normal operation conditions. Thus, the GFM in VIC mode still acts as a voltage source without directly controlling the output current, and grid-synchronization is achieved by PSC throughout the grid fault period. It should be noted that the design of magnitude and phase angle of virtual impedance has considerable effects on the inrush current limitation effect and transient stability capability of the GFM [13].

2.2   Mode-Switching Control (MSC)

When switchers S_1–S_3 are chosen at 2, MSC will be adopted to realize FRT control. The operation principle

for MSC is that, when there is a grid fault, the GFM will be switched to the DC control mode to directly regulate the output current using a trip signal. Thereafter, it is necessary to switch back to normal operation control to realize power regulation using a reset signal after fault clearance. This mode switching adds difficulties in control system implementation. In the DC control mode, the reference current of DC control can be derived as follows:

$$\begin{cases} I_{dref} = I_d^* = I_{abc}\sin\delta, \\ I_{qref} = I_q^* = I_{abc}\cos\delta, \end{cases} \qquad (4)$$

where I_d^* and I_q^* are the reference output current in dq frame. I_{abc} and δ are the current amplitude and power angle. The current injection of the GFM during grid fault periods must meet the grid-code requirements to support grid recovery and maintain transient stability simultaneously. It should be noted that a GFM under MSC synchronizes with the grid using PLL during grid fault periods, while re-synchronization is determined by the dynamic response of PSC.

2.3   Current Limiting Control (CLC)

When switchers S_1–S_3 are chosen at 3, an instantaneous current limiter will be triggered to limit the output current without changing the outer voltage controller, as depicted in Fig. 1. Since the cascaded control loop is inherently equipped with a current limiter, there is no need to detect the fault to give a signal to activate the FRT control strategy. Under this condition, the reference angle of the GFM is still derived from the PSC loop. The mathematical model in CLC mode can be described as follows:

$$\begin{aligned} I_{\lim d} &= \begin{cases} I_{dref}^*, & \text{Logic} = 1, \\ \sqrt{I_{\max}^2 - I_{ref}^2}, & \text{Logic} = 3, \end{cases} \\ I_{\lim q} &= \begin{cases} I_{qref}^*, & \text{Logic} = 1, \\ -I_{ref}, & \text{Logic} = 3, \end{cases} \end{aligned} \qquad (5)$$

where $I_{\max}$ and I_{ref} are the maximum output current and reference current of the current limiter, respectively. I_{dref}^* and I_{qref}^* represent the active and reactive reference current delivered from outer voltage control loop, respectively. The current limiter directly provides maximum reactive current, and active current value is derived accordingly to avoid an additional output fault current.

3   Comparison of transient inrush current elimination

Since GFMs are controlled to mimic the dynamic response of SGs, output characteristics are similar to those of a controlled voltage source. When the GFM is subjected to grid faults, transient inrush current will occur

Table 1   The corresponding relationship between the switcher and FRT control

Switchers S_1–S_3	1	2	3
FRT control strategy	VIC	MSC	CLC

due to interactions between two voltage sources. According to Ref. [1], the fault current of the GFM can be divided into two parts: periodic AC component i_p and aperiodic DC component i_{ap}, which can be described as follows:

$$i_p = \sqrt{2} \frac{|E - V'_g|}{Z'_{eq}} \sin(\omega t + \varphi'), \tag{6}$$

$$i_{ap} = \left[\sqrt{2} \frac{|E - V_g|}{Z_{eq}} \sin(\omega t_0 + \varphi) - \sqrt{2} \frac{|E - V'_g|}{Z'_{eq}} \sin(\omega t_0 + \varphi') \right] e^{-\frac{t}{T_a}}, \tag{7}$$

where E, V_g, and V'_g are the output voltage phasor of the GFM as well as grid voltage phasor before and during fault conditions, respectively. Z_{eq} and Z'_{eq} represent the equivalent impedance before and during fault conditions, respectively. $T_a = L'/R'$, T_a is the time constant of the free damping part, and L' and R' represent the total inductance and resistance, respectively. φ is the angle difference between phasor E and V_g, while φ' represents the angle difference between phasor E and V'_g. It can be observed from Eq. (6) that the periodic AC component is determined by the voltage difference and equivalent line impedance. The aperiodic DC component only depends on the instantaneous voltage difference at the fault occurring time and will attenuate to zero after a certain time constant.

When VIC is adopted, the GFM operates in the voltage control mode, and transient inrush current can still be divided into two parts. Although additional virtual impedance can reduce the periodic AC component, the aperiodic DC component cannot be regulated directly, which can only be damped by choosing proper virtual resistance and inductance to change attenuation time constant T_a. When MSC or CLC is adopted, the output

characteristics of the GFM is similar to an equivalent current source during grid fault periods, as illustrated in Figs. 3(b) and 3(c). Thus, for a GFM in MSC and CLC mode, the output current can be restricted directly and transient inrush current can be eliminated effectively. It should be noted that both MSC and VIC implementation rely on instant grounded fault detection to trigger FRT control strategies, whereas CLC is inherently adopted in voltage/current control loops and no triggering signal is needed, as shown in Fig. 3. The intuitive current limitation comparison is summarized in Table 2.

To give intuitive comparison of current limitation, simulation results of a GFM with different FRT control strategies are shown in Fig. 4. The simulation model was established in PSCAD/EMTDC. The topology of the system is shown in Fig. 2, and the detailed parameters are presented in Table 3. The operation condition requires that there be a three-phase grounded fault at 2 s and the grid voltage dips to 30% of the rated value. Detailed simulation results are shown in Fig. 4. It can be observed from Fig. 4(a) that the peak fault current of a GFM in VIC mode will reach four times the rated value, which is much higher than that of a GFM with CLC and MSC. However, MSC will result in current distortion during the first cycle of the grid fault due to control-strategy switching, as shown in Fig. 4(b). Furthermore, CLC shows good performances in current limitation, as shown in Fig. 4(c). During the actual implementation of FRT control, there will be certain time delay before the FRT control is activated, since fault-detection time delay is inevitable. When time delays of 0.005 s or 0.01 s are considered, the effect of the current elimination under VIC will deteriorate remarkably, as shown in Fig. 4(a). However, transient inrush current elimination under CLC is effective, as indicated in Fig. 4(c).
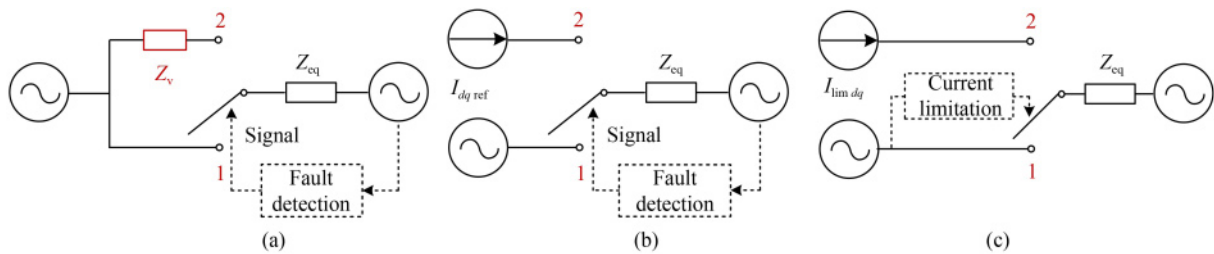
Fig. 3 Equivalent model of a GFM when different FRT control strategies are adopted.
(a) Virtual impedance control (VIC); (b) mode-switching control (MSC); (c) current limiter control (CLC).

Table 2 Transient current elimination of GFMs with different FRT control strategies

Fault current characteristics	VIC	MSC	CLC
Triggering signal	Yes	Yes	No
Equivalent source	Voltage source	Current source	Current source
Periodic AC component	decreased	Direct current control	Direct current control
Aperiodic DC component	Limited effect	None	None

4 Comparison of transient synchronization stability capability

It is important for the GFM to remain synchronized with the grid during grid faults and to realize re-synchronization with the grid after fault clearance. As indicated in previous studies, transient synchronization stability is mainly dominated by the transient response of synchronization control loops [22]. PSC and PLL are commonly used to realize synchronization among VSCs and the grid, while there are intrinsic differences in the stability mechanism between PSC and PLL. The detailed control topology of PSC and PLL can be found in Fig. 5. The transient stability of PSC is accomplished by active power balance, while voltage balance determines whether PLL control can reach a stable point [6]. At different stages during the FRT process, the transient stability of the GFM is determined by different synchronization control loops. The detailed analysis are as follows.

Under normal operation conditions, the GFM synchro-nizes with the grid using the PSC loop. The mathematical model of the PSC loop can be described by the swing equation, as shown by Eq. (1), and the transient stability of PSC loop can be determined using EAC theory. The stability criterion can be described by the P-δ curve, as shown in Fig. 6(a). Curve I represents P-δ characteristics before grounded fault, while curves II and III illustrate P-δ characteristics in under-fault and post-fault situations, respectively. The maximum output active power is denoted as P_{max1}, P_{max2}, and P_{max3}. During fault periods, there are two possible operation states according to the voltage drop depth. One condition is that P_{max2} is larger than reference active power P_0 so that the VSG can reach a stable equilibrium during the fault period. The other condition is that P_{max2} is smaller than reference active power P_0 and no stable equilibrium point can be reached during fault period. According to EAC theory, whether a GFM can maintain transient stability depends on the size of acceleration area S_1 and deceleration area S_2. When the fault is cleared at δ_c, the maximum angle reached by the GFM is denoted as δ_{max}. The maximum angle δ_{max} can be
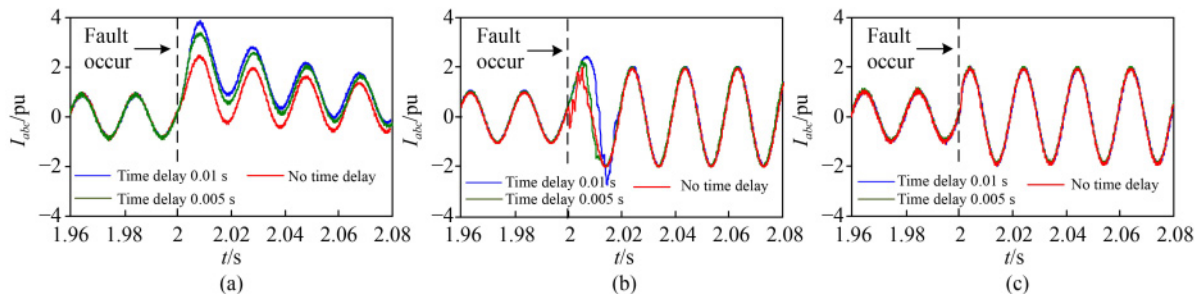
Fig. 4 Time-domain simulation results of a GFM with different time delays.
(a) VIC; (b) MSC; (c) CLC.

Table 3 Detailed parameters of the grid-connected GFM

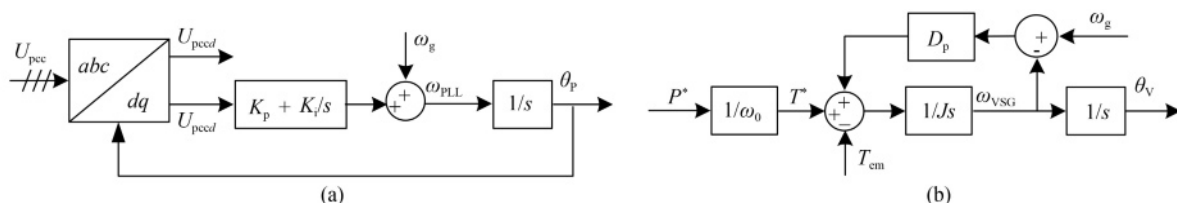| Parameter	Value	Parameter	Value	Parameter	Value
V_{dc}/V	1000	$P_0 + jQ_0$/kVA	20 + j5	K_p	20
E_0/V_g/V	311/311	ω_0/(rad·s^{-1})	314.15	K_i	400
J	5.0224	K	32	I_{max}/A	100
D	8	$R_2 + jX_2$/Ω	0.314 + j0.785	I_{ref}/A	30
D_q	166.7	$R_1 + jX_1$/Ω	0.314 + j0.314	I^*_{dref} and I^*_{qref}/A	80
L_f/C_f	3 mH/40 µF	Z_v/Ω	0.157 + j1.57	I^*_{qref}/A	60

Fig. 5 Control topology of different synchronization control strategies.
(a) PLL; (b) PSC.

calculated using $S_1 = S_2$. When δ_{max} is smaller than unstable equilibrium point δ^u, the GFM is considered stable. Otherwise, the GFM is considered unstable.

4.1 Transient stability mechanism with VIC

When VIC is adopted, virtual impedance will be added during grid fault periods, while PSC is responsible for grid-synchronization throughout the FRT process, and the GFM remains in voltage control mode. By substituting Eq. (3) into Eq. (1), the swing equation of the GFM with virtual impedance can be calculated as follows:

$$J\frac{d\omega}{dt} = \left(T_0 - \frac{V_{abc}^2 G}{\omega_0}\right) - \frac{V_{abc} V_g}{|Z_{eq}+Z_v|\omega_0}\sin\left(\delta+\theta-\frac{\pi}{2}\right) - D_p(\omega-\omega_0),$$
(8)

where G and θ are the conductance and total line impedance angle, respectively. Define $T_1 = T_0 - V_{abc}^2 G/\omega_0$, which refers to the reference torque. It can be observed from Eq. (8) that maximum active power output P_{em} is reduced when additional virtual impedance is considered. Under this condition, acceleration area S_1 (red dotted line) will increase and deceleration area S_2 (blue dotted line) will decrease, as illustrated in Fig. 6(a). Therefore, the transient stability of a GFM with VIC will deteriorate. However, according to Eq. (8), reference torque T_1 may decrease when a suitable virtual impedance angle is

selected to increase total conductance G. This means that, if the virtual impedance presents resistive characteristics, the reference active power will reduce from P_0 to P_{01}, as illustrated in Fig. 7(a). Under this condition, acceleration area S_1 will decrease and deceleration area S_2 will increase, which can benefit the transient stability of the GFM. Furthermore, the resistor would provide additional energy damping, which helps to stabilize the GFM.

4.2 Transient stability mechanism with MSC

When MSC is adopted, the GFM would be controlled as a current source using PLL to realize synchronization during grid fault periods. The PLL control diagram is based on synchronous reference frame PLL (SRF-PLL), as illustrated in Fig. 5(a), which can be modeled as follows:

$$\theta_{PLL} = \int [\omega_0 + (K_p U_{pccq} + K_i \int U_{pccq}dt)]dt,$$
(9)

where θ_{PLL} is the output angle of PLL and U_{pccq} represents the q axis component of the point of common coupling (PCC) voltage. K_p and K_i are the proportional and integral coefficients, respectively. The q axis component of the PCC voltage can be calculated as follows:

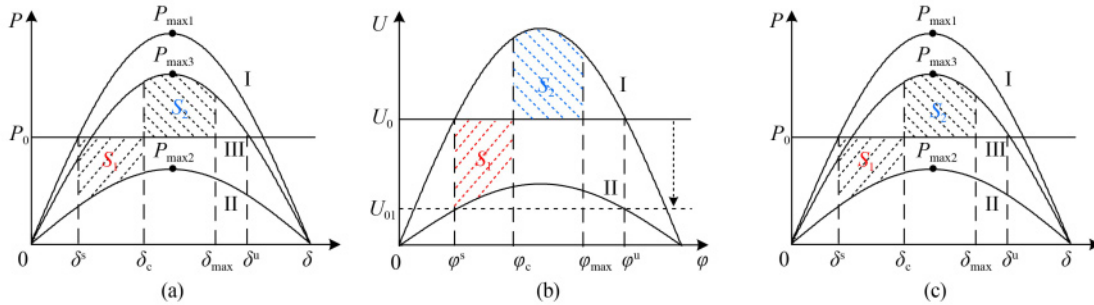$$U_{pccq} = I_d X_2 + I_q R_2 - U_g \sin\varphi,$$
(10)

Fig. 6 Transient stability mechanism of a GFM under different FRT control modes.
(a) VIC; (b) MSC; (c) CLC.

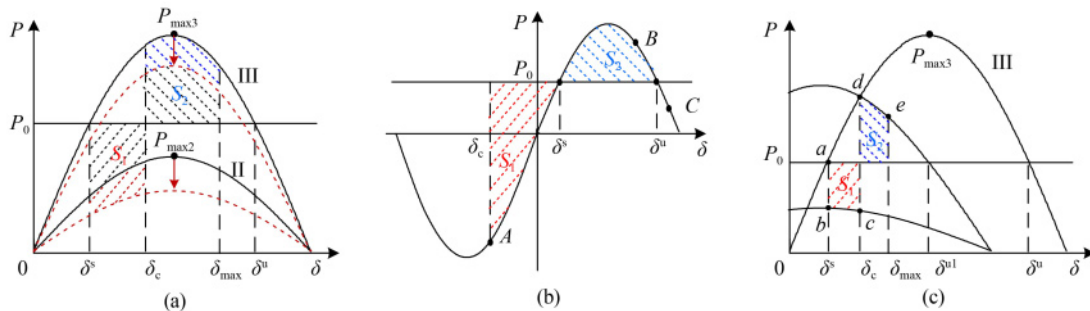**Fig. 7** Design-oriented transient stability analysis of the GFM.
(a) VIC; (b) MSC; (c) CLC.

where $\varphi = \theta_{PLL} - \theta_g$ and θ_g is the grid angle. I_d and I_q represent the active and reactive current components, respectively; X_2 and R_2 are the equivalent reactance and resistance between the PCC and grid, respectively. Substituting Eq. (10) into Eq. (9) yields the following:

$$\varphi = \int \left[\left(K_p + K_i \int \right) (I_d X_2 + I_q R_2 - U_g \sin\varphi) \right] \mathrm{d}t. \quad (11)$$

Furthermore, the second-order derivation of both sides of Eq. (11) can be described as follows [22]:

$$J_L \frac{\mathrm{d}^2\varphi}{\mathrm{d}t^2} = U_0 - U_g \sin\varphi - D(\varphi) \frac{\mathrm{d}\varphi}{\mathrm{d}t}, \quad (12)$$

where equivalent inertia J_L, equivalent reference voltage U_0, and damping coefficient $D(\varphi)$ can be defined as follows:

$$\begin{cases} J_L = \dfrac{1 - K_p I_d L_2}{K_i}, \\ U_0 = I_d X_2 + I_q R_2, \\ D(\phi) = \dfrac{K_p}{K_i} U_g \cos\phi. \end{cases} \quad (13)$$

By comparing Eq. (12) and Eq. (1), it can be observed that the mathematical model of GFMs in both PLC and PSC modes can be equivalent to the swing equation of the SG. Based on the derived models, transient instability mechanism in PLL mode can also be explored in the U-φ domain using EAC theory, as illustrated in Fig. 6(b). Curves I and II represent the voltage curve $U_0\sin\varphi$ during and after a grounded fault, respectively. Due to the voltage imbalance during grid fault periods, the state variables of the GFM will change with curve II. If there is a stable equilibrium point between reference voltage U_0 and $U_0\sin\varphi$, the GFM can maintain stability during grid fault periods, as shown by line U_{01} in Fig. 6(b). If there is no stable equilibrium point, the GFM will lose synchronization without islanding the fault location. According to EAC theory, when $S_1 = S_2$, the GFM will reach maximum angle difference φ_{max}. If φ_{max} is smaller than unstable equilibrium point (UEP) φ^u, the GFM operation can remain stable. Different from SGs, reference voltage U_0 is adjustable and is determined by the injection current (I_d/I_q) and line impedance (R_2/X_2). Thus, it is feasible to improve transient stability by injecting a suitable current to reduce U_0 to U_{01}.

When the control system is switched back to PSC mode, the transient stability mechanism is determined by the swing equation and is shown in Fig. 6(b). The difference is that the initial operating point may not be the stable equilibrium point, and there are three possible conditions that need to be discussed. The first condition is that angle difference δ decreases to a negative value, as shown by point A. Under this condition, ω would increase due to power imbalance. The critical criterion for transient stability is that $S_1 < S_2 + S_D$, where S_D is the dissipation energy. The second condition is that δ increases to point B, which is smaller than unstable

equilibrium point δ^u. Under this condition, ω would decrease and δ probably exceed stable point δ^s and reach the negative half of the axis. However, it is clear that the acceleration area is smaller than the deceleration area, indicating that the VSG can reach a stable point. The third condition is that the GFM operates at point C, which implies that δ exceeds δ^u. Under this condition, the operation point of the VSG would diverge and cannot reach a stable operation point. Thus, it can be concluded that whether a GFM under MSC can realize re-synchronization with the grid is determined by the initial operating point.

Based on the transient mechanism analysis, a proper control design can help to improve the transient stability of a GFM under MSC mode. Since the transient stability of the PLL loop is determined by the voltage balance according to Eq. (10), transient enhancement control can be achieved by adjusting current injection angle to reduce $U_0 = I_d X_2 + I_q R_2$ to a certain value, as shown in Fig. 7(b). According to EAC theory, the reduction of U_0 can benefit the transient stability of the GFM during grid fault periods. For a purely resistive network, if only reactive current is injected, U_0 equals to 0, which can guarantee the existence of stable equilibrium point during grid fault periods.

4.3 Transient stability mechanism with CLC

When CLC is adopted, the GFM would be triggered into current control mode with PSC to realize synchronization with the grid. Under this condition, the output current is determined by Eq. (5), and the voltage controller would be out of loop. θ is defined as the output current angle and it equals to arctan($I_{\lim q}/I_{\lim d}$). By ignoring the power loss caused by the filter and line impedance, the output active power of the GFM in CLC mode can be calculated as follows [18].

$$P_{CLC} = V_g I_{max} \cos(\delta - \theta) = P_{\lim max} \cos(\delta - \theta). \quad (14)$$

According to Eq. (14), the P-δ domain curve can be redrawn as shown in Fig. 6(c), and the transient stability criterion is different from that under other FRT control strategies. When there is a grounded fault, the GFM will be driven into current-limitation mode and the operating point will shift from a to b. Due to the power imbalance, the angular frequency will increase to point c until the grid fault is cleared. Since the angular frequency is larger than the rated value, the operating point will move from d to e till the angular frequency is smaller than the rated value. Under this condition, the maximum angle value is denoted as δ_{max}. If δ_{max} is smaller than unstable equilibrium point δ^{u1}, the GFM is considered stable. Otherwise, the GFM will enter an unstable region. The stable operation region of the GFM under CLC is remarkably smaller compared with that under normal operation conditions because δ^{u1} is much smaller than δ^u.

Based on the instability mechanism analysis, a proper control design can benefit the transient stability of the GFM under CLC mode. As illustrated in Fig. 7(c), when the GFM steps into current limitation mode, the P-δ curve is dominated by the cosine function. The pre-set current angle θ would have a considerable effect on the transient stability, as shown by Eq. (14). Compared with the condition that θ equals to 0, a positive value can cause the curve to shift to the right. Under this condition, acceleration area S_1 would decrease, whereas deceleration area S_2 increases, which would help to stabilize the GFM.

4.4   Transient sability estimation and simulation validation

To validate the correctness of the theoretical analysis, simulation results based on PSCAD/EMTDC are presented in this Section. The topology of the established model is the same as that in Fig. 2, and detailed parameters of the system are shown in Table 3. The operation principle is that when a grounded fault occurs, three different FRT control strategies are triggered to limit the fault current to realize FRT. After fault clearance, VIC will be activated to be out of loop and MSC would be switched to the normal control scheme. However, CLC will remain in maximum output-current-limitation mode. In the following section, two simulation cases are presented to validate the correctness of the theoretical analysis.

Case I: The first simulation case is that the three-phase grid voltage dips to 30% of the rated value at 1 s and the fault is cleared at 1.9 s. Additional impedance Z_v under VIC and the reference output current under MSC and CLC are shown in Table 3. The simulation results are shown in Fig. 8.

It can be observed from Fig. 8(a) that, when VIC is adopted, the PSC module is responsible for realizing synchronization with the grid throughout the fault process. When the fault is cleared at 1.9 s, the angle difference δ of GFM reaches approximately 180°, which is larger than unstable equilibrium point δ^u, as illustrated in Fig. 6(a). Under this condition, the angle difference δ is prone to diverge, which would result in an oscillation of the output current. Furthermore, the power output fluctuation would lead to an oscillation of the output voltage through the Q-V droop control loop. As shown in Fig. 8(a), the transient instability phenomenon of the GFM is the same with that of SGs. When MSC is adopted, the GFM will rely on the PLL module to realize synchronization during grid faults. It can be observed in Fig. 8(b) that the GFM has already lost transient stability during the grid fault period. Under this condition, the amplitude of output current is determined by the reference current, while the angle derived from PLL module will change, resulting in output voltage oscillation, as illustrated in Fig. 8(b). After fault clearance, it can be observed from Fig. 8(b) that the initial power angle of the GFM is at approximately 170°, which is larger than the UEP in Fig. 6(b). Under this condition, the GFM will diverge and cannot return to a stable state. The transient stability is dominated by the PSC module, and the transient instability phenomenon is the same as that shown in Fig. 8(a). Compared with VIC and CLC, there is control-mode switching under MSC, which makes MSC more complicated in terms of its control design. Moreover, the GFM under PLL mode acts as a current source without frequency regulation ability in islanding mode. When CLC is triggered, the output current of the GFM will be limited to the maximum value automatically. When the fault is cleared at 1.9 s, the power angle of the GFM reaches approximately 300°,
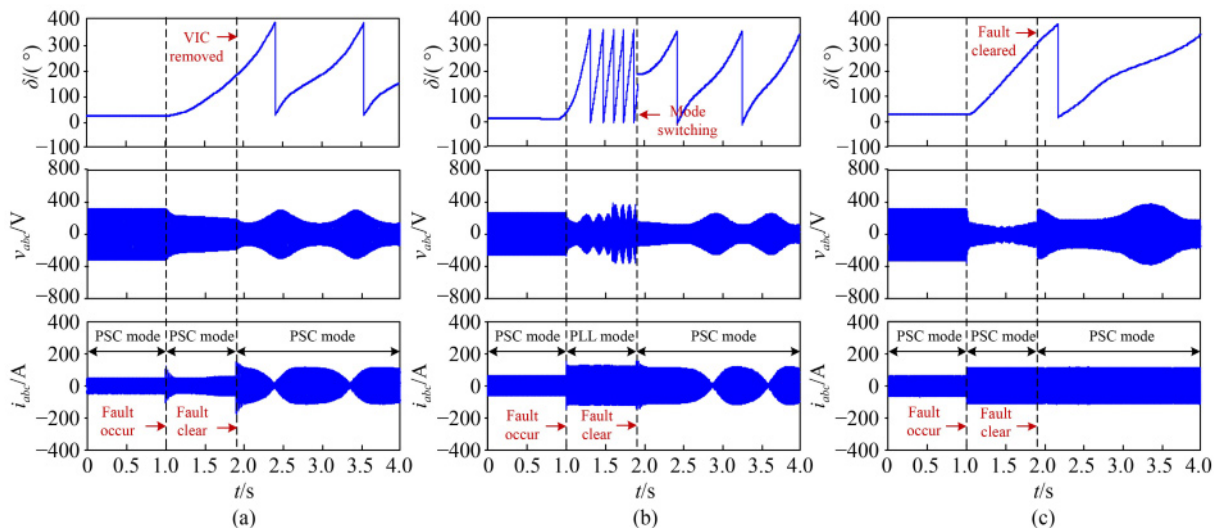
Fig. 8   Transient instability phenomenon of a GFM with different FRT control strategies when the grounded fault is cleared at 1.9 s.
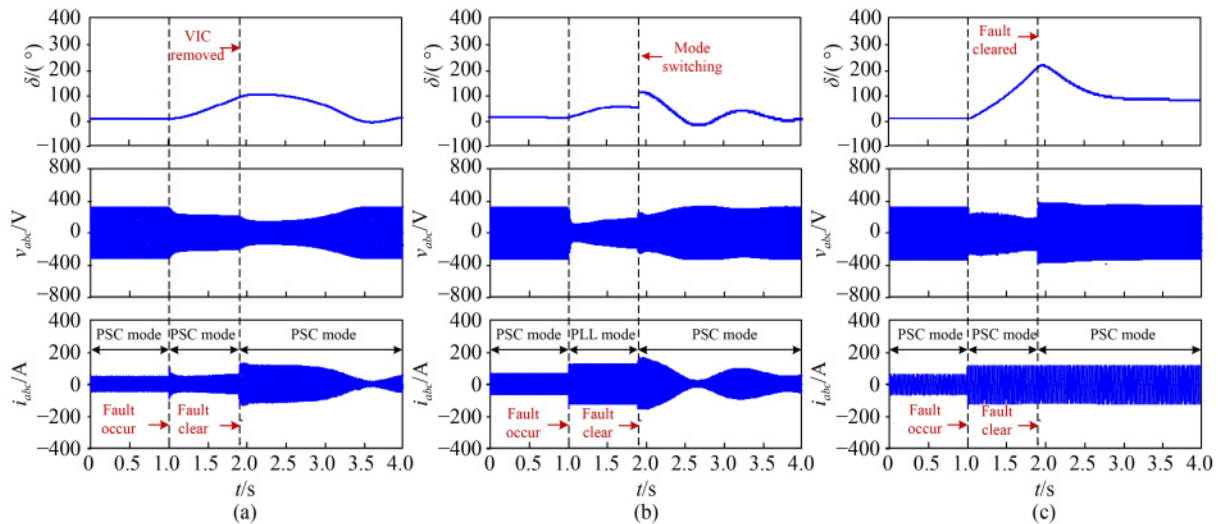(a) VIC; (b) MSC; (c) CLC.

which is much larger than the UEP in Fig. 6(c). Under this condition, the GFM will lose transient stability and the power angle will diverge, as shown in Fig. 8(c). However, the amplitude of the output current remains constant, whereas the variation of current phasor angle will lead to a fluctuation of the output voltage, as depicted in Fig. 8(c).

Case II: The second simulation case is that the three-phase grid voltage drops to 30% of the rated value at 1 s and the fault is cleared at 1.9 s. However, additional impedance Z_v under VIC equals to 0.5 + j0.05 pu. The reference currents I_{dref}^* and I_{qref}^* under MSC are 0 A and 100 A, respectively, and the initial operation point is controlled to reach the stable equilibrium point. Furthermore, reference active current I_{ref} under CLC is set to 60 A, and the maximum current value is 100 A.

It can be observed from Fig. 9 that, when control parameters of VIC, MSC, and CLC are re-designed, the GFM can maintain transient stability throughout the fault period. As indicated in Fig. 9(a), the angle difference δ would return to its normal value after fault clearance. For

MSC, the GFM can maintain stability in both the PLL and PSC modes since the initial operation point at fault clearing time is set to be close to the stable equilibrium point. The results show the correctness of theoretical analysis of the transient stability mechanism of the GFM with different control strategies.

To provide an intuitive illustration of Cases I and II in the ω-δ domain, phase portrait simulation results are presented, as shown in Fig. 10. It can be observed in Fig. 10(a) that state variables would diverge to infinite in Case I, whereas the system can return to the equilibrium point in Case II. In Fig. 10(b), the transient stability of the GFM in the PLL control mode during grounded fault is shown. In Case I, the GFM would lose transient stability, which is consistent with the time-domain simulation results shown in Fig. 8. In Case II, the GFM can maintain synchronization, whereas the power angle is not at the equilibrium when the fault is cleared, as shown in Fig. 9(b). In Fig. 10(c), the state variables of the GFM diverge and cannot reach a stable operation point in Case I. In Case II, the system can reach a stable state. The

Fig. 9 Simulation results of a GFM with different FRT control strategies when detailed control parameters are re-designed. (a) VIC; (b) MSC; (c) CLC.
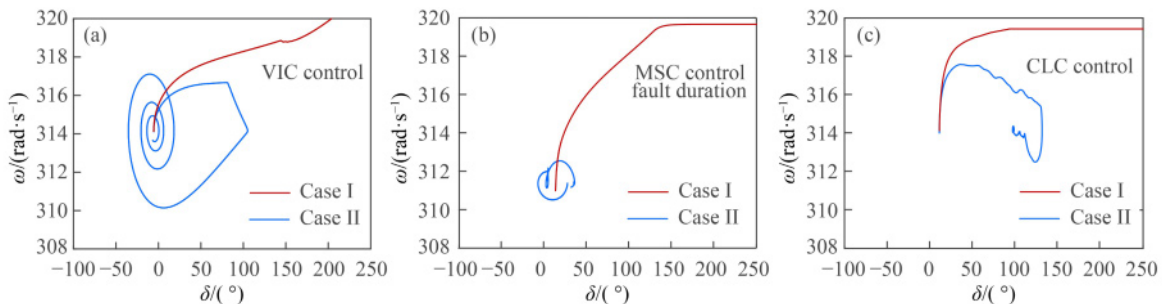

Fig. 10 Simulation results of a GFM with phase portrait in the ω-δ domain when different FRT control strategies are considered. (a) VIC; (b) MSC; (c) CLC.

phase portrait simulation results are consistent with time-domain simulation results.

Transient current limitation was compared in the previous section, and a theoretical analysis of the transient stability mechanism is presented in this Section. To guide the choice of FRT control strategies under different operation conditions, the sensitivity of the FRT control strategies to the short circuit ratio (SCR) of the grid are be compared using the critical clearance time (CCT) in the following section [6]. The simulation results for CCT versus SCR domain are shown in Fig. 11. It should be noted that the calculation of CCT is based on the established model with same system parameters and control parameters, except the SCR. It can be observed from Fig. 11 that, when the SCR increases from 4 to 32, the CCT of the GFM under VIC increases from 0.53 s to 0.68 s, whereas the CCT of the GFM under CLC remains almost constant at 0.09 s. The results indicate that, compared with CLC, VIC is more sensitive to changes in the SCR. Furthermore, when the SCR increases from 4 to 12, the CCT of the GFM under MSC changes from 0.27 s to 0.7 s. It is clear that the SCR has the greatest effect on MSC, since the PLL module dominates the transient stability of the GFM during grid faults. According to the theoretical analysis and simulation results presented above, the transient stability comparison of a GFM under three different control strategies can be concluded as shown in Table 4.
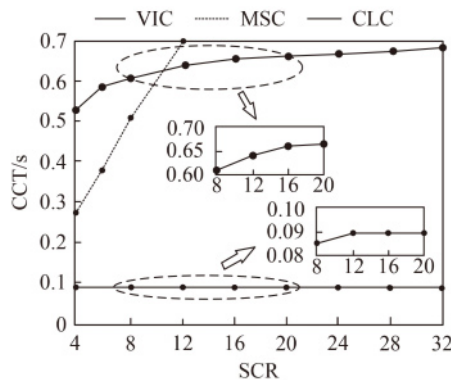
Fig. 11 Relationship between the CCT and SCR. (The bold solid line is the CCT under VIC, the dashed line is the CCT under MSC, and the solid line is the CCT under CLC.)

Table 4 Transient stability comparison throughout FRT process

FRT control	Before fault occurring	During fault period	After fault clearance	Frequency regulation	Re-synchronization complexity	Sensitivity to SCR
VIC	PSC	PSC	PSC	Yes	Low	Medium
MSC	PSC	PLL	PSC	No	High	High
CLC	PSC	PSC	PSC	Yes	Medium	Low

5 Conclusions

This paper investigates the transient performance of GFMs with different FRT control strategies. In particular, transient inrush current and transient synchronization stability issues are featured and an intuitive comparison is presented. Detailed conclusions can be made as follows.

(1) From the perspective of inrush current limitation, the transient inrush current of the GFM can be divided into periodic AC and aperiodic DC. When VIC is adopted, the GFM remains in voltage-control mode, and additional virtual impedance can effectively limit the periodic AC component, whereas the aperiodic DC component remains uncontrollable. This is not beneficial for current limitation when time delay is considered. However, both CLC and MSC would turn the GFM into current control mode, which can regulate output current directly. Thus, they have good current limitation performance even when time delay is considered.

(2) Based on the transient stability analysis, both VIC and CLC realize synchronization with the grid using PSC throughout the fault period, whereas MSC would rely on PLL to synchronize with grid during grid faults and changes to a PSC-dominant mode after fault clearance. This makes the control design of MSC more complicated. Furthermore, MSC is more sensitive to the SCR of the system due to the existence of a PLL, which means that it is prone to instability issues when subjected to extremely weak system conditions. However, The CCT of VIC and CLC changes within a small range when there is a significant change in the SCR of the system.

References

1. Shuai Z K, Shen C, Yin X, et al. Fault analysis of inverter-interfaced distributed generators with different control schemes. IEEE Transactions on Power Delivery, 2018, 33(3): 1223–1235

2. Vandoorn T L, De Kooning J D M, Meersman B, et al. Review of primary control strategies for islanded microgrids with power-electronic interfaces. Renewable & Sustainable Energy Reviews, 2013, 19: 613–628

3. Rathnayake D B, Akrami M, Phurailatpam C, et al. Grid forming inverter modeling, control, and applications. IEEE Access: Practical Innovations, Open Solutions, 2021, 9: 114781–114807

4. Zhong Q C, Weiss G. Synchronverters: inverters that mimic synchronous generators. IEEE Transactions on Industrial Electronics, 2011, 58(4): 1259–1267

5. Wu H, Ruan X, Yang D, et al. Small-signal modeling and parameters design for virtual synchronous generators. IEEE Transactions on Industrial Electronics, 2016, 63(7): 4292–4303

6. Shen C, Shuai Z K, Shen Y, et al. Transient stability and current

injection design of paralleled current-controlled VSCs and virtual synchronous generators. IEEE Transactions on Smart Grid, 2021, 12(2): 1118–1134

7. Shuai Z K, Shen C, Liu X, et al. Transient angle stability of virtual synchronous generators using Lyapunov's direct method. IEEE Transactions on Smart Grid, 2019, 10(4): 4648–4661

8. E. ON Netz Gmbh. Grid code—high and extra high voltage. Bayreuth, 2006

9. Japanese Grid—Interconnection Code, 2012, document JEAC 9701–2012, addendum-2012-No.1

10. He X Q, Geng H, Li R, et al. Transient stability analysis and enhancement of renewable energy conversion system during LVRT. IEEE Transactions on Sustainable Energy, 2020, 11(3): 1612–1623

11. Shuai Z K, Huang W, Shen C, et al. Characteristics and restraining method of fast transient inrush fault currents in synchronverters. IEEE Transactions on Industrial Electronics, 2017, 64(9): 7487–7497

12. Sadeghkhani I, Hamedani Golshan M E, Guerrero J M, et al. A current limiting strategy to improve fault ride-through of inverter interfaced autonomous microgrids. IEEE Transactions on Smart Grid, 2017, 8(5): 2138–2148

13. He J W, Li Y W. Analysis, design, and implementation of virtual impedance for power electronics interfaced distributed generation. IEEE Transactions on Industry Applications, 2011, 47(6): 2525–2538

14. Lu X N, Wang J, Guerrero J M, et al. Virtual-impedance-based fault current limiters for inverter dominated AC microgrids. IEEE Transactions on Smart Grid, 2018, 9(3): 1599–1612

15. Zhang W, Rocabert J, Candela J I, et al. Synchronous power control of grid-connected power converters under asymmetrical grid fault. Energies, 2017, 10(7): 950

16. B. Rathore, S. Chakrabarti, L. Srivastava. A self-regulated virtual impedance control of VSG in a microgrid. Electric Power Systems Research, 2021, 197: 107289

17. Bottrell N, Green T C. Comparison of current-limiting strategies during fault ride-through of inverters to prevent latch-up and wind-up. IEEE Transactions on Power Electronics, 2014, 29(7): 3786–3797

18. Xin H H, Huang L B, Zhang L, et al. Synchronous instability mechanism of P-f droop-controlled voltage source converter caused by current saturation. IEEE Transactions on Power Systems, 2016, 31(6): 5206–5207

19. Jongudomkarn J, Liu J, Ise T. Virtual synchronous generator control with reliable fault ride-through ability: a solution based on finite-set model predictive control. IEEE Journal of Emerging and Selected Topics in Power Electronics, 2020, 8(4): 3811–3824

20. Moon M S, Johnson R W. DSP control of UPS inverter with overcurrent limit using droop method. In: 30th Annual IEEE Power Electronics Specialists Conference, Charleston, USA, 1999

21. Barsali S, Ceraolo M, Pelacchi P, et al. Control techniques of dispersed generators to improve the continuity of electricity supply. In: 2002 IEEE Power Engineering Society Winter Meeting, New York, USA, 2002

22. Taul M G, Golestan S, Wang X, et al. Modeling of converter synchronization stability under grid faults: the general case. IEEE Journal of Emerging and Selected Topics in Power Electronics, 2022, 10(3): 2790–2804